ORIGINAL ARTICLE

Spatial evaluation of climate change-induced drought characteristics in different climates based on De Martonne Aridity Index in Iran

Mohammad Jafarpour[1] · Arash Adib[1] · Morteza Lotfirad[1] · Özgur Kisi[2]

Abstract

In recent years, greenhouse gas emissions have caused extensive changes in the global climate. Climate change leads to extreme events, such as droughts. The present study investigates precipitation and temperature variations and the past and future drought characteristics in Iran through data from 40 synoptic stations and 33 general circulation models (GCMs) under RCP4.5 and RCP8.5 scenarios. As a first step, the country of Iran was classified into different climatic regions based on De Martonne aridity index. The GCMs were ranked using TOPSIS in four climatic regions and an ensemble of top ten GCMs was used in each region. Furthermore, the homogeneity of monthly precipitation was studied in the baseline and future periods. Meteorological drought was calculated through the standardized precipitation index (SPI), deriving drought severity, peak, and duration based on run theory. The results revealed that precipitation will reduce in future periods in the majority of Iran and temperature will reduce in the south and southeast and will increase in the northwest and north of Iran. Furthermore, the highest drought severity and peaks will occur in semi-arid and arid regions, while the longest drought duration will happen in the southeast and west of Iran. Overall, future droughts are found to have higher severity, duration, peaks, and standard deviation than the baseline period. Also, the results showed a reducing trend of the SPI values in northwestern regions, while the other stations indicated no significant trend.

Introduction

Although the emissions of greenhouse gases (GHG), e.g., CO_2, began in the late nineteenth century, such emissions have rapidly increased in the past 50 years on account of the accelerated industrialization of countries. Increased GHG emissions raise the air temperature over time, leading to climate change and global warming (Esmaeili-Gisavandani et al. 2021). Climate change observations in many countries have shown that this phenomenon leads to reduced precipitation in semi-arid and arid climates and increased precipitation in humid climates (Feng et al. 2014). For example, Sahour et al. (2020) showed increased aridity (decreased precipitation and increased evaporation) in most Middle

Eastern countries from 1948 to 2018, and My et al. (2022) showed an increasing trend of temperature and a decreasing trend of winter precipitation in southern Italy (with a Mediterranean climate) from 1956 to 2019. In mountainous regions, precipitation increases, but evaporation and aridity decrease (Zhang et al. 2023).

Arid and semi-arid climates account for the majority of Iran. Numerous studies focused on climate change outcomes in Iran through the outputs of GCMs, e.g., climate change impacts on precipitation and temperature.

Abarghouei et al. (2011) studied the drought trend and variations in different parts of Iran. The results indicated a reducing trend of drought in many Iranian regions, particularly the southeast, western, and southwestern parts. They reported that drought severity had increased in most regions in the past 30 years. Tabari et al. (2012) investigated precipitation and drought severity of 10 synoptic stations in the east of Iran during 1966–2005. The results revealed that precipitation and drought variation severity increased with aridity in the south of the case study region. All the studied stations experienced at least one severe drought in the

✉ Arash Adib
arashadib@yahoo.com

1 Civil Engineering and Architecture Faculty, Shahid Chamran University of Ahvaz, Ahvaz, Iran

2 Civil Engineering Department, School of Technology, Ilia State University, Tbilisi, Georgia

study period, most of which occurred in winter. Golian et al. (2015) examined agricultural and meteorological droughts and their trends in 6 provinces of Iran from 1980 to 2013. They used the standardized precipitation index (SPI) and standardized streamflow index (SSI) for agricultural and meteorological droughts and the multivariate standardized drought index (MSDI) for meteorological-agricultural droughts. A significant reduction was observed in the precipitations of the northern, northwestern, and central parts at a confidence level of 95%. Dashtpagerdi et al. (2015) studied drought severity and magnitude based on SPI in different periods at 25 synoptic meteorological stations in arid and semi-arid Iranian regions during 1975–2005. They demonstrated that, in general, the arid and semi-arid regions of Iran had reducing SPI trends and increasing droughts. Najafi and Moazami (2016) analyzed precipitation trends and the frequency and magnitude of extreme precipitations in Iran during 1969–2009 using 187 gauging stations. The results showed a reducing trend of annual precipitation, particularly in the north, west, and northwest of Iran. According to the results, the northwest of Iran had a reducing trend not only in precipitation but also in the frequency and magnitude of extreme precipitations. Zarei and Eslamian (2017) studied the precipitation trend and SPI using meteorological data from 20 synoptic stations in the south of Iran during 1985–2013. They identified two drought periods, including 1998–2003 and 2010–2012. Also, it was found that precipitation had reducing trends in spring and winter. Alizadeh-Choobari and Najafi (2018) investigated climate change and its impacts on some extreme meteorological events using daily temperature and precipitation data during 1951–2013. They reported that Iran temperature increased by 1.3 °C in this period. Also, they reported an increasing trend of hot events and a reducing trend of cold events. Precipitation declined by 8 mm per decade due to the greater transmission of water vapor in subequatorial regions to higher latitudes before the formation of precipitation. Darand and Sohrabi (2018) identified and evaluated the drought- and flood-prone regions by analyzing the daily precipitation variations of 1437 stations in Iran from 1962 to 2013. They showed that the northwest, arid, and semi-arid regions of Iran were most likely to experience droughts. Abbasian et al. (2019) evaluated the performance of general circulation models (GCMs) in the simulation of temperature and precipitation in Iran during 1901–2005. They employed Climatic Research Unit (CRU) data as the baseline dataset. The results suggested the higher performance of GCMs in temperature simulation than in precipitation simulation in Iran. The models CMCC-CMS and MRI-CGCM3 were found to have the highest performance in temperature and precipitation simulation. Vaghefi et al. (2019) utilized the minimum/maximum temperature and precipitation distribution of 122 stations for the baseline of 1980–2004 and projected extreme

temperature and precipitation events and six large resulting flash flood events. They employed five GCMs in simulation. The results implied a climate with long-scale droughts and fluctuating severe precipitations, suggesting that some regions in Iran might become uninhabitable. Sharafati et al. (2020) calculated SPI and identified drought characteristics of 102 synoptic stations in Iran. They studied the trends of the drought characteristics in different climates in Iran. They observed that short-term droughts (≤ 6 months) were more severe in the north and northwest of Iran, while long-term droughts (> 6 months) were more severe in the southern, southwestern, and southeastern regions. Also, the northwest of Iran was more sensitive to drought severity, duration, and peak. Doulabian et al. (2021) exploited 6 synoptic stations in Iran and investigated the impacts of climate change on precipitation and temperature using 25 GCMs under scenarios RCP2.6, RCP4.5, and RCP8.5. The results showed increased temperatures in all the regions and all the months; however, precipitation was found to fluctuate. They suggested that it was important to select an ensemble of GCMs to examine hydroclimatic changes.

There are many studies which investigated the impact of climate change on precipitation and temperature (Adib and Marashi 2019; Mo et al. 2019; Ghasemi et al. 2022; Dlamini et al. 2022), runoff (Ahmadianfar and Zamani 2020; Adib et al. 2021; Ghafouri-Azar et al. 2021; Lotfirad et al. 2022a), groundwater (Sharma et al. 2015; Jeihouni et al. 2019), flood (Modarres et al. 2016; Maghsood et al. 2019), drought (Bahrami et al. 2019) and crop yield (Chen et al. 2013; Vaghefi et al. 2015; Hadinia et al. 2017). In this study, 33 GCMs were used to assess the impact of climate change on precipitation and temperature in Iran. A major innovation in this study is the climate zoning of Iran and the selection of the best GCMs using TOPSIS in each climate region. The trend and characteristics of future droughts in each zone are calculated. It is vital to understand meteorological droughts, precipitation, and temperature variations, as well as drought trends and characteristics for making effective policy decisions in Iran in future.

The phases of the present research include: (1) evaluating the performance of 33 GCMs based on the AR5 report in the simulation of rainfall and temperature in the baseline period of 1966–2005, (2) classifying Iran into four climates based on the De Martonne climatic classification, (3) selecting the top ten GCMs in each climate using the TOPSIS multi-criteria decision analysis, (4) using the ensembles of the top GCMs of each climate, (5) extracting the climatic variables of the top GCMs in future period under the scenarios RCP4.5 and RCP8.5, (6) utilizing the change factor method (CFM) to downscale the temperature and precipitation variables, (7) calculating SPI in future and baseline periods under the scenarios RCP4.5 and RCP8.5, (8) identifying drought characteristics, e.g., severity, peak, and duration in

future and baseline periods, and (9) investigating the spatial variation trends of the drought characteristics in future and baseline periods.

Materials and methods

Case study

Iran is situated in Southwest Asia with an area of 1,648,195 km^2. Iran has different climates due to its extensive area covering different latitudes and elevations, the presence of the Alborz and Zagros Mountains in the north and west of the country, respectively, and large deserts in the central and eastern parts. Overall, the dominant climate of Iran is arid and semi-arid as it is located in the arid belt of the Northern Hemisphere. The annual mean precipitation and temperature are 235.2 mm and 15.82 °C respectively.

Data and analysis

Climatic data

The present study utilized monthly precipitation and temperature data (prepared by the Iran Meteorological Organization) from 40 synoptic stations throughout Iran (Fig. 1) during 1966–2005 as the baseline period (Table 1). A few gaps in the precipitation time series were reconstructed using the CRU re-analysis database. In fact, the number of missing data was negligible and data integrity was not compromised. The maximum number of missing data is 3 months at Bam station from January to March 2004 (due to the earthquake).

De Martonne climatic classification

The De Martonne aridity index is based on the aridity index $I = P/(T + 10)$, in which T is the average temperature (°C), while P is the average annual precipitation in mm (Rahimi et al 2013). The gridded precipitation and temperature data of the CRU TS4.03 in the NetCDF format with the spatial resolution of 0.5° from 1966 to 2005 were extracted for Iran using ArcGIS V.10.2. The temperatures and precipitations of CRU cells were compared with those of the corresponding synoptic stations. CRU data are gridded. Therefore, the validity of the data of each cell can be compared with the data of the station located inside the desired cell (Jafarpour et al. 2022).

GCM outputs

33 GCMs of the inter-government panel on climate change (IPCC) the coupled model inter-comparison project—phase 5 (CMIP5) with a spatial resolution of 0.5° were subjected to bias correction (BCSD) which is a trend-preserving

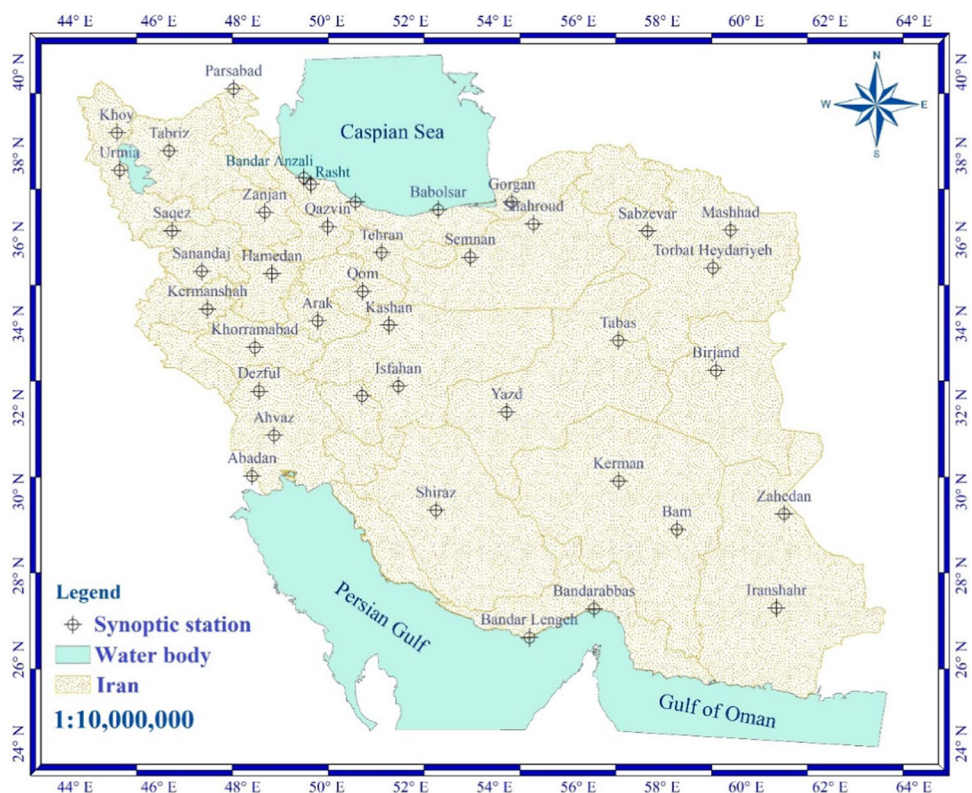**Fig. 1** Location of stations used in this study

Table 1 Stations' specifications

Station	Lat	Lon	Elevation (m)	P Mean (mm)	T Mean (°C)	Station	Lat	Lon	Elevation (m)	P Mean (mm)	T Mean (°C)
Abadan	30.38	48.21	6.6	157.48	25.79	Urmia	37.66	45.06	1328	330.80	11.25
Ahvaz	31.34	48.74	22.5	231.60	26.16	Parsabad	39.60	47.78	72.6	289.96	14.84
Arak	34.07	49.78	1702.8	326.06	13.93	Qazvin	36.32	50.02	1279.1	317.50	14.16
Babolsar	36.72	52.65	−21	911.45	17.06	Qom	34.77	50.86	879.1	146.00	18.32
Bam	29.10	58.35	1066.9	57.61	23.62	Ramsar	36.90	50.68	−20	1230.12	16.16
Bandarabbas	27.21	56.37	9.8	168.56	27.04	Rasht	37.32	49.62	−8.6	1344.84	16.20
Bandaranzali	37.48	49.46	−23.6	1762.99	16.38	Sabzevar	36.21	57.65	962	190.21	17.93
Bandarlengeh	26.53	54.83	22.7	132.16	27.67	Sanandaj	35.25	47.01	1373.4	437.59	14.29
Birjand	32.89	59.28	1491	159.83	16.80	Saqez	36.22	46.31	1522.8	483.42	11.98
Dezful	32.40	48.38	143	382.71	24.27	Semnan	35.59	53.42	1127	139.07	18.41
Esfahan	32.52	51.71	1550.4	127.67	16.68	Shahrekord	32.29	50.84	2048.9	320.36	12.26
Gorgan	36.91	54.41	0.0	564.40	17.59	Shahrud	36.38	54.93	1325.2	160.19	14.78
Hamedan	35.20	48.69	1679.7	322.46	11.25	Shiraz	29.56	52.60	1488	314.81	18.32
Iranshahr	27.23	60.72	591.1	108.67	27.54	Tabas	33.60	56.95	711	82.19	22.62
Kashan	33.97	51.48	955	132.47	19.83	Tabriz	38.12	46.24	1361	275.03	12.54
Kerman	30.26	56.96	1754	133.67	17.16	Tehran	35.69	51.31	1191	235.82	17.71
KermanShah	34.35	47.15	1318.5	444.55	15.03	Torbatheydarieh	35.33	59.21	1451	255.20	14.71
Khoy	38.56	45.00	1103.4	293.13	12.76	Yazd	31.90	54.29	1230	56.57	19.83
Khoramabad	33.44	48.28	1147.8	499.30	17.28	Zahedan	29.47	60.90	1370	78.00	18.92
Mashhad	36.24	59.63	999.2	250.07	14.60	Zanjan	36.66	48.52	1659.4	301.85	11.43

statistical downscaling algorithm, which has been widely used to generate accurate and high-resolution data sets (Abatzoglou and Brown 2012). The website of http://gdo-dcp.ucllnl.org was used for downloading of data. The periods of 1966–2005 and 2030–2069 were applied (the future period under the scenarios of RCP4.5 and RCP8.5). These NetCDF data were extracted in ArcGIS V.10.2.

Performance criteria

So as to evaluate the efficiency of the GCMs in precipitation simulation, the long-term precipitation data of the GCMs during 1966–2005 were compared to the baseline precipitation data of the synoptic data through five common criteria, including Pearson's correlation coefficient (R), Nash–Sutcliffe efficiency (NSE), Taylor skill score (S_{T}), root-mean-square error (RMSE), and mean absolute percentage error (MAPE). Lower RMSE and MAPE values and closer R, NS, and S_{T} values to 1 would imply more realistic GCM precipitation projections. The evaluation criteria are:

$$R = \frac{\sum\limits_{i=1}^{n}\left(X_{\mathrm{Cal}}^{i} - \overline{X}_{\mathrm{Cal}}\right)\left(X_{\mathrm{Obs}}^{i} - \overline{X}_{\mathrm{Obs}}\right)}{\sqrt{\sum\limits_{i=1}^{n}\left(X_{\mathrm{Cal}}^{i} - \overline{X}_{\mathrm{Cal}}\right)^{2}}\sqrt{\sum\limits_{i=1}^{n}\left(X_{\mathrm{Obs}}^{i} - \overline{X}_{\mathrm{Obs}}\right)^{2}}} \tag{1}$$

$$\mathrm{RMSE} = \sqrt{\frac{\sum\limits_{i=1}^{n}\left(X_{\mathrm{Obs}}^{i} - X_{\mathrm{Cal}}^{i}\right)^{2}}{n}} \tag{2}$$

$$\mathrm{NS} = 1 - \frac{\sum\limits_{i=1}^{N}\left(X_{\mathrm{Cal}}^{i} - X_{\mathrm{Obs}}^{i}\right)^{2}}{\sum\limits_{i=1}^{N}\left(X_{\mathrm{Obs}}^{i} - \overline{X}_{\mathrm{Obs}}\right)^{2}} \tag{3}$$

$$\mathrm{MAPE} = \frac{1}{n}\sum\limits_{i=1}^{n}\left|\frac{X_{\mathrm{Obs}}^{i} - X_{\mathrm{Cal}}^{i}}{X_{\mathrm{Obs}}^{i}}\right| \times 100 \tag{4}$$

$$S_{T} = \frac{4(1 + R)^{k}}{\left(\sigma + \frac{1}{\sigma}\right)^{2}(1 + R_{0})^{k}} \tag{5}$$

where X_{obs} denotes baseline data, X_{cal} is calculated data, $\overline{X}_{\mathrm{obs}}^{i}$ is the average baseline temperature (precipitation), and n is the number of months. Also, R is the coefficient of correlation between the baseline and calculated data, R_{0} is the maximum theoretical value of the linear correlation coefficient, σ is the ratio of the calculated standard deviation to the baseline standard deviation, and K is the order of formula (recommended to be 4 for the temperature and 2 for precipitation) (Taylor 2001).

TOPSIS ranking of the GCMs

Hwang and Yoon (1981) proposed a performance ranking technique. The technique operates on the grounds of mutual difference. Hence, the best alternative is the lowest difference from the ideal solution and the highest difference from the non-ideal solution. After performing the De Martonne aridity index and evaluating the precipitation of the period of the GCMs based on the baseline precipitation during 1966–2005, the GCMs were ranked in the four climates based on TOPSIS. TOPSIS has been employed in many hydrological and climate change studies (see Farajpanah et al. 2020; Zamani and Berndtsson 2019).

GCMs ensemble

As mentioned, a period of 2030–2069 was considered as the future period. To minimize uncertainty-induced errors in climate change research, one should not use a single model and a single scenario. Depending on the research objectives, at least two models and several scenarios should be employed. Using of different GCMs can reduce the created uncertainty by a single GCM (Gholami et al. 2023).

A larger model weight in simulations represents a smaller uncertainty-induced error. The present study adopted the combined weighting of the GCMs.

$$g_{1} = R(P_{\mathrm{GCM}}, P_{\mathrm{obs}}) \tag{6}$$

$$g_{2} = R(T_{\mathrm{GCM}}, T_{\mathrm{obs}}) \tag{7}$$

$$g_{3} = \frac{\sigma(P_{\mathrm{obs}})}{\mathrm{RMSE}(P_{\mathrm{obs}})} \tag{8}$$

$$g_{4} = \frac{\sigma(T_{\mathrm{obs}})}{\mathrm{RMSE}(T_{\mathrm{obs}})} \tag{9}$$

$$g_{5} = \left[1 - \left(\frac{|R(P_{\mathrm{obs}}, T_{\mathrm{obs}}) - R(P_{\mathrm{GCM}} - T_{\mathrm{GCM}})|}{2}\right)\right] \tag{10}$$

where R is the linear correlation coefficient, $\sigma(P_{\mathrm{obs}})$ is the baseline precipitation standard deviation, $\sigma(T_{\mathrm{obs}})$ is the baseline temperature standard deviation, P_{obs} is the baseline precipitation, T_{obs} is the baseline temperature, P_{GCM} denotes the GCM precipitation, and T_{GCM} stands for the GCM temperature. The values of g_{1}–g_{5} were calculated for each model, weighting the models as:

$$w_i = g_1 \times g_2 \times g_3 \times g_4 \times g_5 \qquad (11)$$

Finally, the average simulated variables (precipitation and temperature) can be obtained using the model weights and model ensembles as:

$$\overline{X} = \frac{\sum_i W_i X_i}{\sum_i W_i} \qquad (12)$$

where i represents the models, W is the model weight, and $\overline{X}$ is the average projected variable (precipitation or temperature) of the model ensemble (Coppola et al. 2010).

Change factor method

Once the data of the GCM models had been extracted in ArcMap, the change factor method (CFM) was employed based on the long-term average precipitation and temperature data of the models. To calculate climate change in each model, the average monthly temperature difference (Eq. 13) and precipitation ratio (Eq. 14) were calculated for the future (2030–2069) and baseline (1966–2005) periods:

$$\Delta T_i = \left(\overline{T}^{future}_{GCM_i} - \overline{T}^{base}_{GCM_i} \right) \qquad (13)$$

$$\Delta P_i = \left(\frac{\overline{P}^{future}_{GCM_i}}{\overline{P}^{base}_{GCM_i}} \right) \qquad (14)$$

where ΔP_i and ΔT_i represent the precipitation and temperature climate change scenarios for the average long-term values of forty years, respectively, $\overline{T}^{future}_{GCM_i}$ and $\overline{P}^{future}_{GCM_i}$ stand for the average simulated future temperature and precipitation, respectively, and $\overline{T}^{base}_{GCM_i}$ and $\overline{P}^{base}_{GCM_i}$ are the average simulated baseline temperature and precipitation, respectively.

Once the time-series of the future climatic scenarios had been obtained, the baseline climate change scenarios (1996–2005) were added:

$$T_{i,j} = T_{obs_{i,j}} + \Delta T_i \qquad (15)$$

$$P_{i,j} = P_{obs_{i,j}} \times \Delta P_i \qquad (16)$$

where $T_{i,j}$ denotes the projected future temperature, $P_{i,j}$ represents the projected future precipitation, $T_{obs_{ij}}$ is the baseline temperature, and $P_{obs_{ij}}$ is the baseline precipitation (Ashofteh et al. 2013).

The values of ΔP_i and ΔT_i are shown for several synoptic stations under RCP4.5 and RCP8.5 scenarios (Figs. 2 and 3).
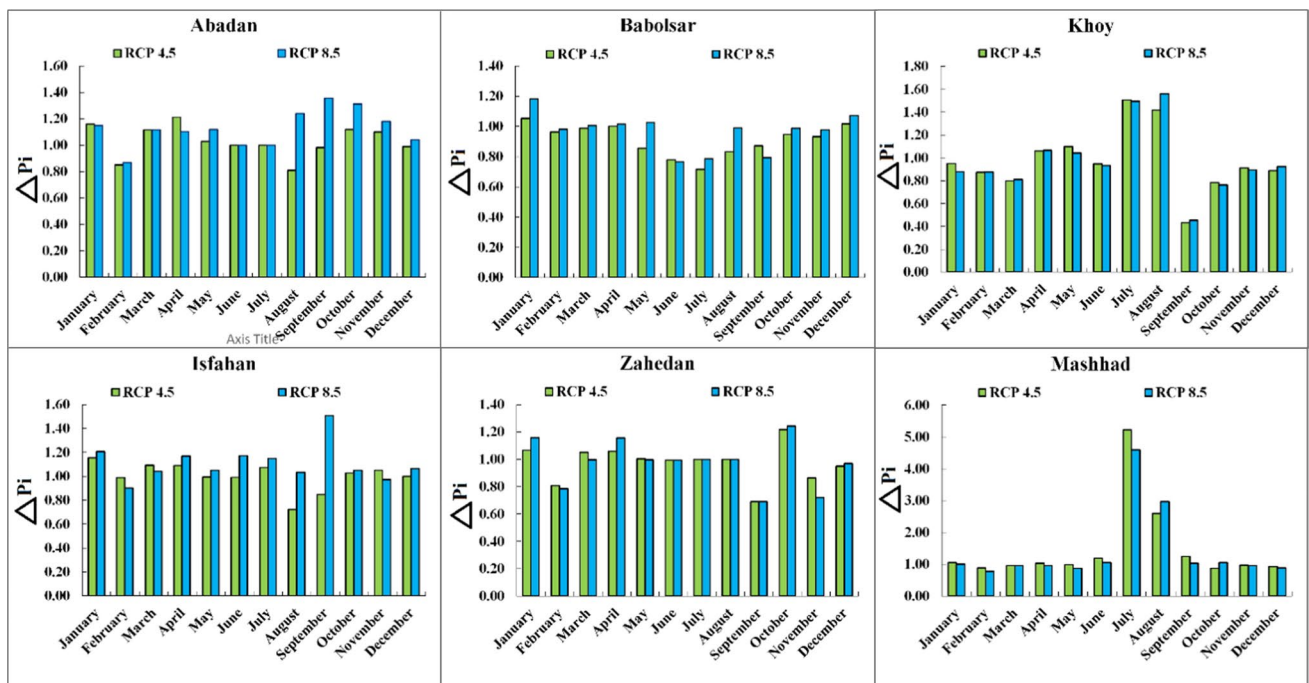

Fig. 2 The value of ΔP_i for several synoptic stations under RCP4.5 and RCP8.5 scenarios in different months
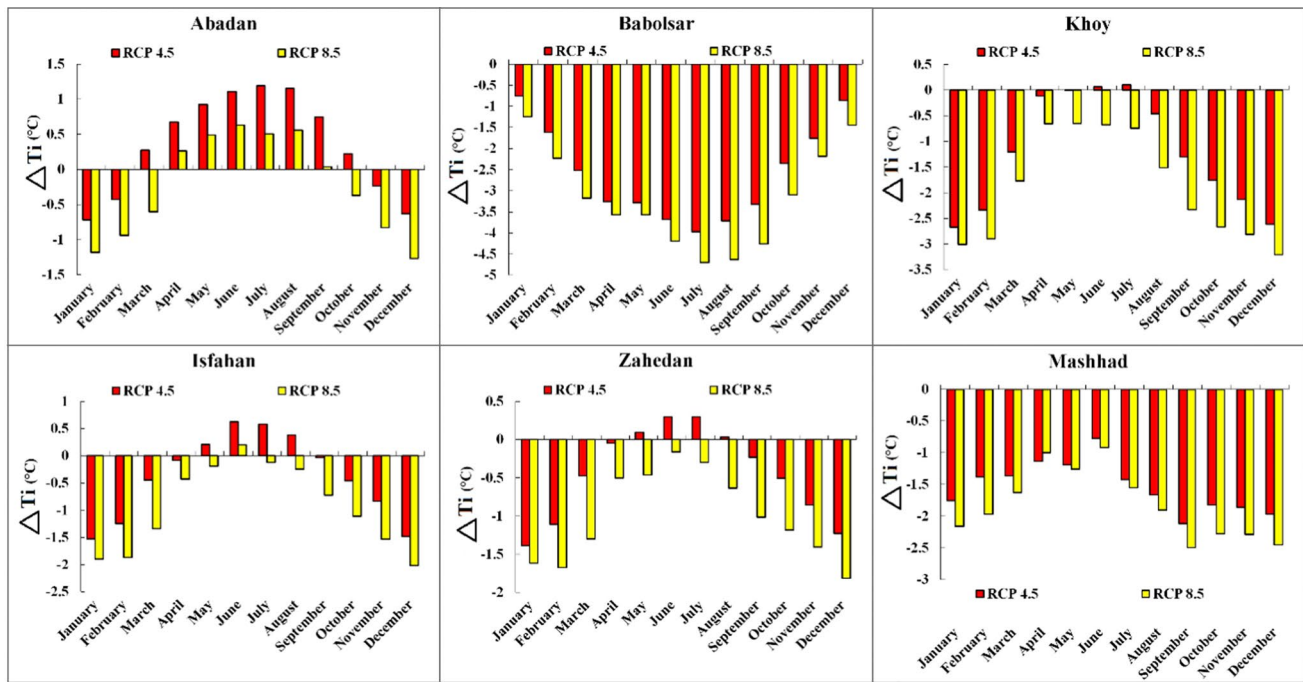
Fig. 3 The value of ΔT_i for several synoptic stations under RCP4.5 and RCP8.5 scenarios in different months

Standardized precipitation index (SPI)

SPI can be calculated for all the regions based on precipitation data. It was proposed by Mckee et al. (1993). To calculate SPI, the gamma probability distribution was used (Tigkas et al. 2015). The gamma distribution was fitted to the monthly precipitation data to calculate SPI. Thom (1958) modified the equation for months with zero precipitation typically occurring in arid and semi-arid climates. SPI was calculated for the future and baseline periods under the scenarios of RCP4.5 and RCP8.5 at a 12-month time scale. Run theory was adopted to analyze the drought characteristics, extracting and examining the duration, severity, and peak of each drought event (Lotfirad et al. 2022b).

Alexanderson's SNHT test

Alexandersson (1986) presented the standard normal homogeneity test (SNHT) to find the variations of monthly precipitation data series. In this test, the t-value modified by Khaliq and Ouarda (2007) is calculated as:

$$
\begin{cases}
T = \max\left[v\overline{Z}_1^2 + (n-v)\overline{Z}_2^2\right] & 1 \leq v < n \\
\overline{Z}_1 = \frac{1}{v}\sum_{i=1}^{v} Z_i \\
\overline{Z}_2 = \frac{1}{n-v}\sum_{i=v+1}^{n} Z_i
\end{cases}
\tag{17}
$$

where n is the number of baseline data points, $\overline{Z}_1$ is the average Z before the variation, $\overline{Z}_2$ is the average Z after the variation, and v is the most probable time of an abrupt change in the data (that is, the last time in the partial time series with an average of Z_1). The present study exploited the SNHT at a confidence level of 95% for 10,000 data points using the Monte Carlo method in order to generate standard random normal numbers (Khaliq and Ouarda 2007). The precipitation time series is homogeneous when the t-value is below the threshold of the 95% confidence level.

Mann–Kendall trend test

Many methods have been introduced to project trends in time series, including the nonparametric Mann–Kendall test. This test was first developed by Mann (1945) and extended by Kendall (1975). This nonparametric method can calculate variations in the time unit. The s-value in the Mann–Kendall test is obtained as:

$$
S = \sum_{i=1}^{n-1} \sum_{j=i+1}^{n} \text{sign}(x_j - x_i)
\tag{18}
$$

$$
\text{Sign}(x_j - x_i) = \begin{cases}
+1 & \text{when}(x_i - x_j) > 0 \\
0 & \text{when}(x_i - x_j) = 0 \\
-1 & \text{when}(x_i - x_j) < 0
\end{cases}
\tag{19}
$$

where x_i is data point i, x_j is data point j, Sign is the sign function, and Z_{MK} indicates the significance of the time series trend as:

$$Z_{MK} = \begin{cases} \frac{S-1}{\sqrt{\text{Var}(S)}} & \text{when } S > 0 \\ 0 & \text{when } S = 0 \\ \frac{S+1}{\sqrt{\text{Var}(S)}} & \text{when } S < 0 \end{cases} \tag{20}$$

In the Mann–Kendall test, Z_{MK} values from -1.96 to 1.96 represent insignificant trends at a confidence level of 95%. Also, $Z_{MK} > 1.96$ and $Z_{MK} < 1.96$ imply increasing and reducing trends at a confidence level of 95%, respectively. To evaluate the trend of SPI, the present study employed the Mann–Kendall test at a 95% confidence level (Lotfirad et al. 2021).

Results

Precipitation data quality of the stations

The monthly precipitation data of the 40 stations suggested homogeneous data in future and baseline periods, according to the SNHT results. Figure 4 depicts the SNHT results of the 40 stations. The red-dotted line represents the SNHT threshold. As can be seen, the t-value is below the threshold at all the stations (the rainfall data of all the stations are homogeneous).

De Martonne classification

The monthly precipitation and temperature data of the baseline period at the studied stations were compared with the CRU re-analysis data. Except for precipitation at the

southern coasts of the Caspian Sea with a perhumid climate, the CRU data had very good performance for the other regions. The results suggest higher performance in temperature simulation than precipitation simulation. As precipitation varies more than temperature, and precipitation doesn't occur every day of the year, the temperature results had a lower degree of uncertainty than precipitation results. Temperature variations occur in a smaller range and are more stable in nature. Furthermore, the temperature can be more easily and accurately measured with lower errors. This is in agreement with the earlier studies (Abbasian et al. 2019; Doulabian et al. 2021). A total of 688 CRU re-analysis cells covered the entire Iran. The zoning map of the De Martonne aridity index was developed using the CRU temperature and precipitation data. The area of Iran was divided into six climates based on the De Martonne classification, including arid, semi-arid, Mediterranean, semi-humid, humid, and perhumid. The 40 stations under study fell in the per-humid, Mediterranean, semi-arid, and arid groups. According to Fig. 5, the majority of Iran has arid and semi-arid climates. Due to this, it is very important to study drought periods and trends in the baseline and future periods.

Selection of the top GCMs via TOPSIS

Prior to the investigation of the future climate change based on GCM simulations, it is important to evaluate the performance of the GCMs in the simulation of climatic variables. It is assumed that GCMs that have a better agreement with base data are assumed to be more accurate when projecting future climatic variables. This has reduced the uncertainty of projections. The present research used the monthly precipitation and temperature data of thirty three GCMs. First, the long-term monthly average temperature and precipitation of the synoptic stations were compared
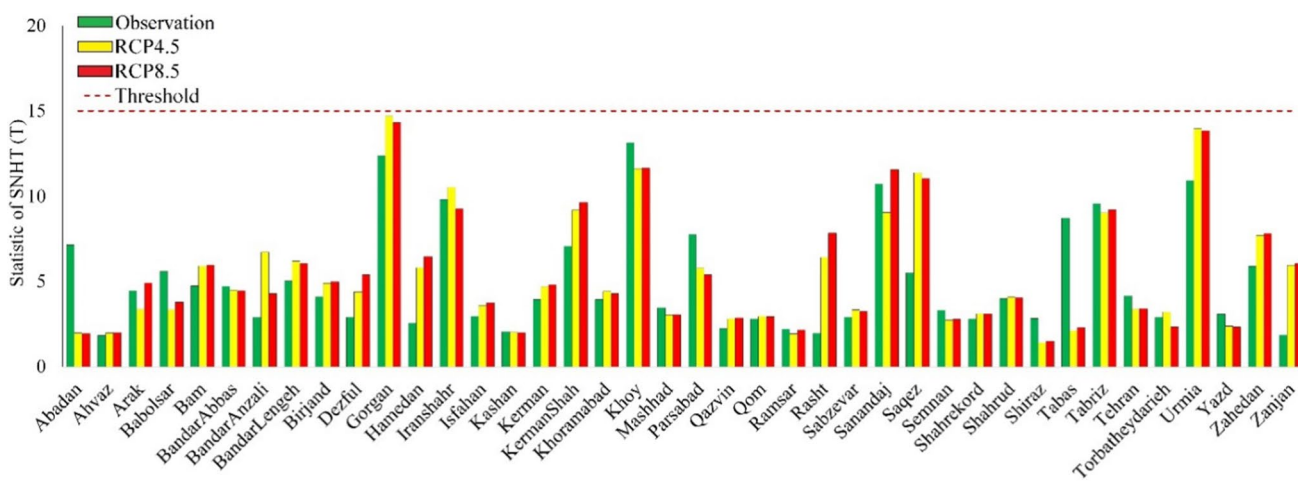

Fig. 4 Homogeneity of precipitation data in future and baseline period with SNHT test

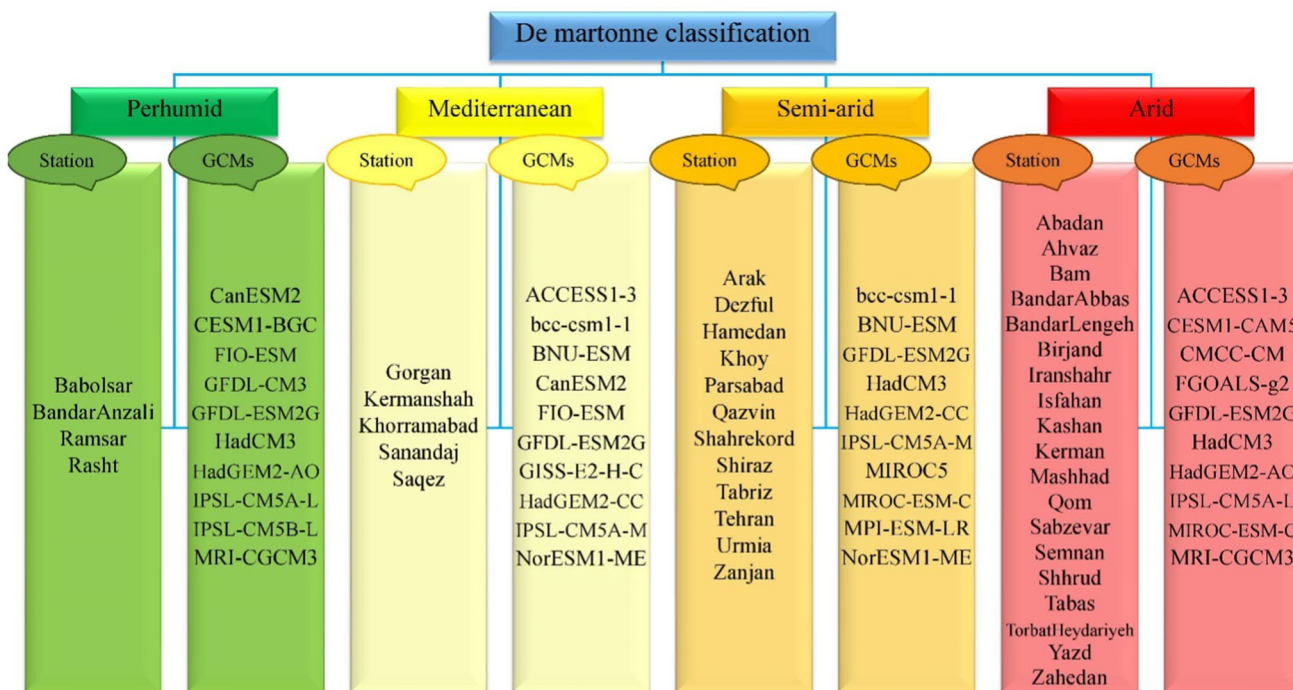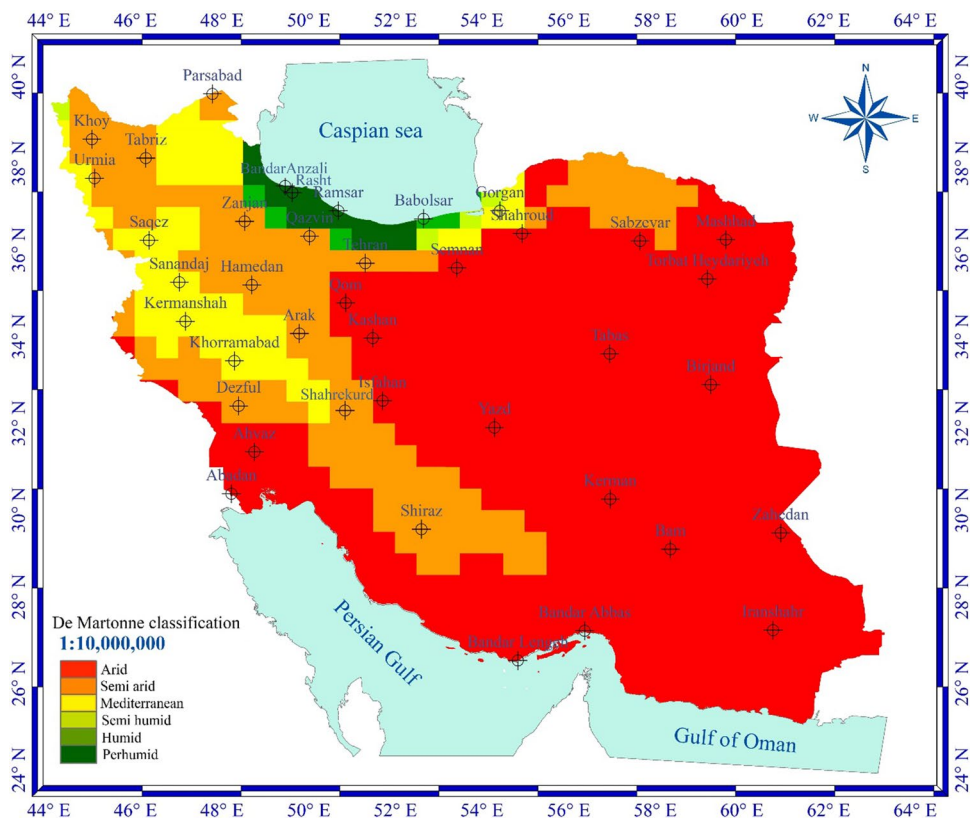**Fig. 5** Climatic classification of Iran according to De Martonne classification

Fig. 6 Selected models in the four climatic zones

with those of the corresponding GCM cells in the baseline period (1966–2005). The GCMs were ranked using TOPSIS based on the performance criteria of RMSE, MAPE, R, NS, and S_T. According to Fig. 5, the stations under study fell into four De Martonne classes. Therefore, ten GCMs with the highest TOPSIS scores (ranks) in these four classes were identified, as shown in Fig. 6.

Future versus baseline temperature and precipitation variations

Once the top ten GCMs had been selected in the climates, their ensembles were used to reduce uncertainty in the climatic simulations. Figures 7, 8 compare the future and baseline temperature and precipitation variations. According to Figs. 7, 8, precipitation rises in the northern regions in winter and spring and reduces in summer and autumn. The opposite is the case with the temperature. This is explained by the high average annual precipitation and humid climate of northern stations, where precipitation decreases to baseline values in spring and summer. It should be noted that the majority of precipitation in northern regions occurred in winter and autumn (over 40% and 30%, respectively), while lower precipitations happened in spring and summer. Also, these regions have a convective precipitation pattern, unlike the other stations.

Spatial distribution of drought characteristics

The descriptive statistics of the drought characteristics were projected for different climates in future and baseline periods, as shown in Figs. 9 and 10. According to Fig. 9, the average drought severity varied from -0.6 to -4.5. In the baseline period, the southeastern and northwestern regions of Iran experienced the largest drought severity. In future period, the drought severity decreases in the southeast and increases in the northwest under both scenarios. Also, the southern regions of Iran and the southern coasts of the Caspian Sea will undergo severe droughts in future. According to Fig. 10, the drought standard deviation varied from 0 to 4. The future drought standard deviations of the northwestern, southern, and southern coasts of the Caspian Sea rise relative to the baseline period, while that of the southeastern part decreases as compared to the baseline period. The southeastern regions will experience reduced average drought peaks in future as compared to the baseline period. Also, the peaks will decline in the central regions and rise in the southern coasts. Furthermore, the drought peak will increase in the northwest corner of Iran in future. The future drought peak standard deviation will reduce in the central and western regions and increase in the northern part relative to the baseline period. According Fig. 10 the standard deviation of drought duration will reduce in the

western coast and increase in the southeastern coast of the Caspian Sea and the northwest corner relative to the baseline period. Also, the standard deviation of future drought duration decreases in the western region while it rises in the northwestern, northern, and southern regions as compared to the baseline period.

Figure 11 shows the spatial distribution of Iran's drought trend based on the Mann–Kendall test. The results revealed a decreasing trend of SPI value in the west, northwest, and, east south coast of the Caspian sea regions in the base period, and no trends were observed for the other stations. It is consistent with the findings of previous studies on drought trends in Iran including (Dashtpagerdi et al. 2015; Golian et al. 2015; Sharafati et al. 2020; Zarei and Eslamian 2017). Also, for the future period, the southeastern region (Zahedan Station) showed a decreasing trend of SPI.

According to Fig. 12, the drought durations are longer in semi-arid and arid climates in the baseline period; the average drought duration of Iran is 2.5–3.5 years. This is also the case with the future period, excluding the Gorgan Station with a Mediterranean climate. The future drought duration of the Gorgan Station was found to be 9–10 years. This can be inferred from the standard deviation values of the drought indices; very humid climates had the lowest standard deviations, while the Mediterranean climates showed the highest standard deviations. The drought peak results show severe droughts in arid climates. As can be seen in Fig. 12, the future period will experience more severe droughts with higher durations, peaks, and standard deviations than the baseline period. These results can be explained by the different rainfall patterns, temperatures, and elevations of the climates. As can be seen in Fig. 5, the northern regions of Iran have a humid climate, low elevations, and very high annual precipitations. The foothills of the Alborz and Zagros mountains have Mediterranean and semi-arid climates, and the western and northwestern regions have a different rainfall pattern from the central regions. For other regions with arid climates, a number of stations lie in the vicinity of deserts and the southern seas (The Persian Gulf and the Gulf of Oman). The regions adjacent to the Gulf of Oman (south and southeast) have a different rainfall pattern from the other regions and experience tropical precipitations in summer. Also, these regions are located at lower latitudes.

Discussion

The comparison of the future annual precipitation to the baseline ones suggests that in all the stations, except for the Dezful and Saqqez stations, precipitation will reduce in future. This is consistent with the earlier works (Alizadeh-Choobari and Najafi 2018). An explanation for these differences can be the overestimates of the GCMs
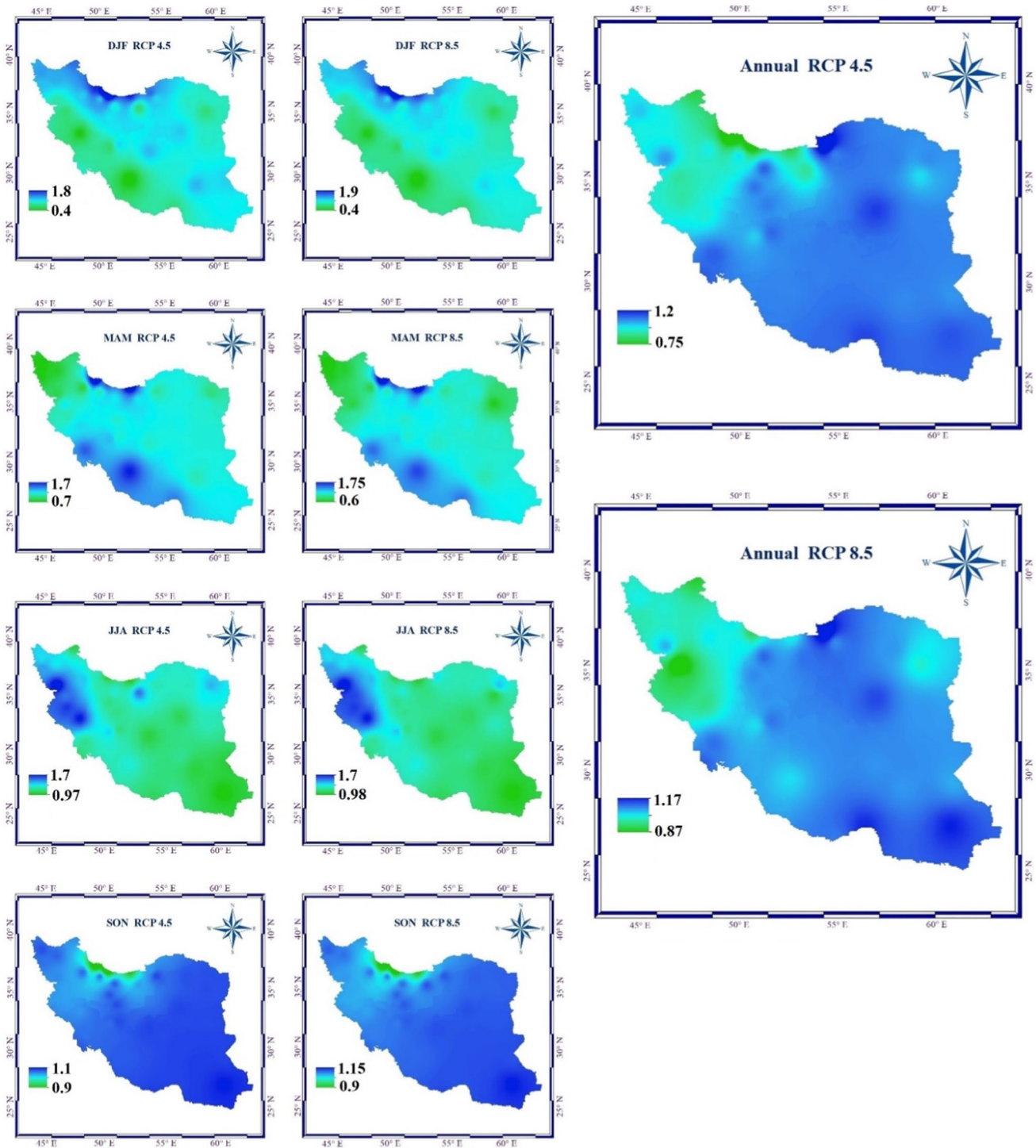
Fig. 7 The ratio of the mean annual and seasonal precipitation under RCP 4.5 and RCP 8.5 scenarios infuture period to the mean annual and seasonal precipitation in the baseline period. (The mean annual precipitation in future period/ the mean annual precipitation in the baseline period) and (the mean seasonal precipitation in future period/ the mean seasonal precipitation in the baseline period). (DJF: December, January, and February; MAM: March, April, and May; JJA: June, July, and August; SON: September, October, and December)
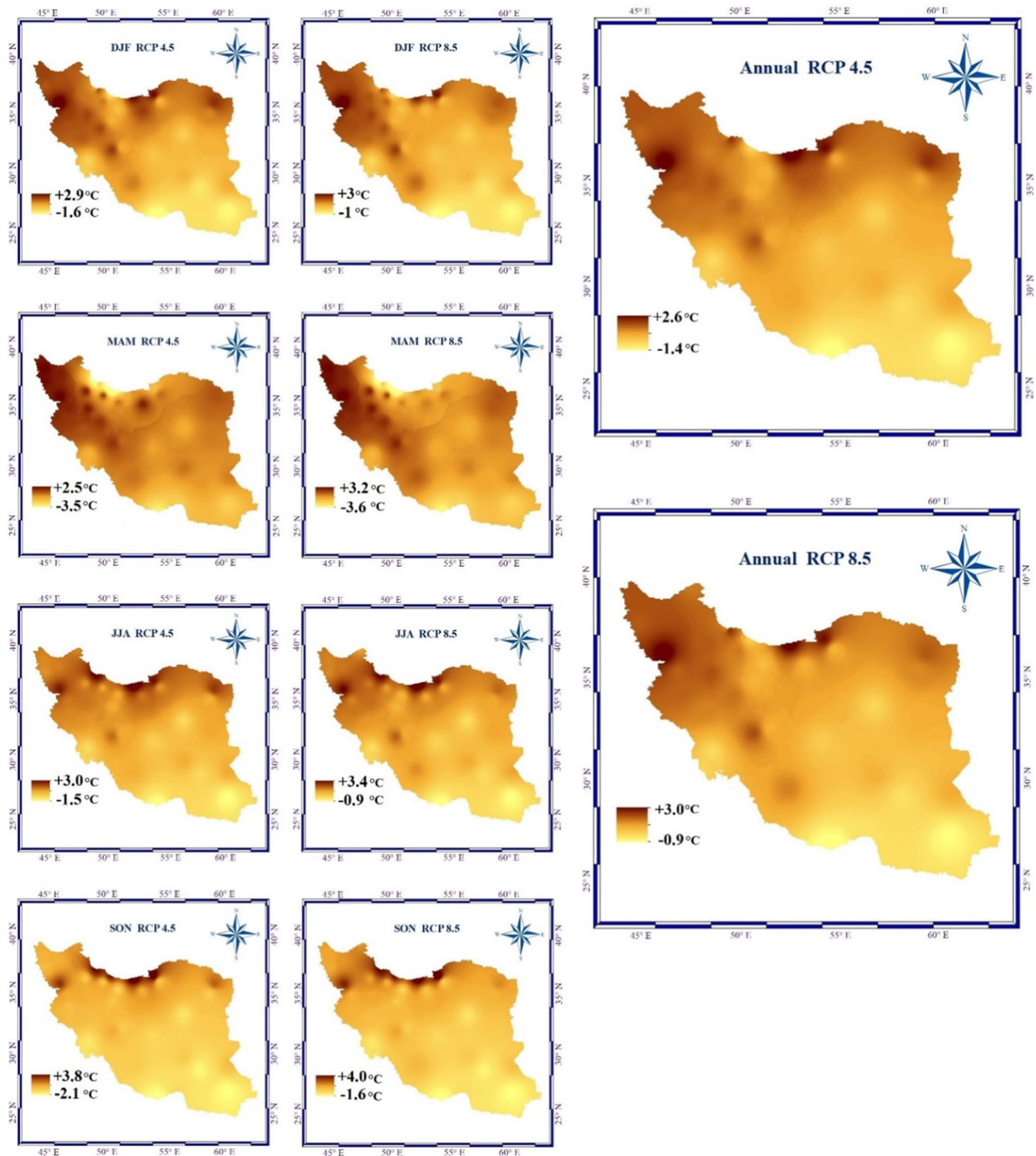
Fig. 8 The difference between the mean annual and seasonal temperature under RCP 4.5 and RCP 8.5 scenarios in future period and the mean annual and seasonal temperature in the baseline period. (The mean annual temperature in future period—the mean annual temperature in the baseline period) and (the mean seasonal temperature in future period—the mean seasonal temperature in the baseline period). (DJF: December, January, and February; MAM: March, April, and May; JJA: June, July, and August; SON: September, October, and December)
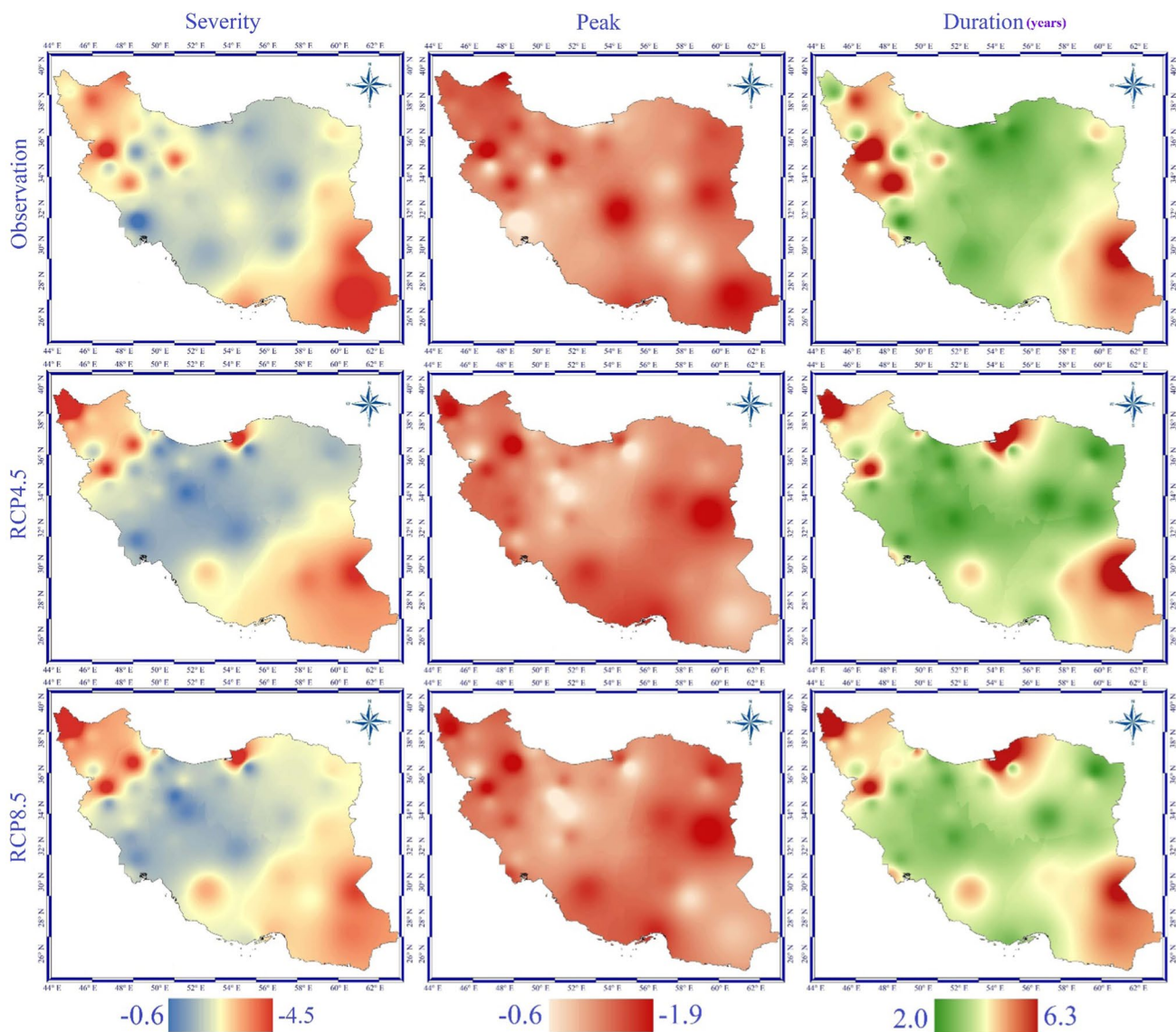
Fig. 9 Spatial distributions of the average drought characteristics

under the scenarios RCP4.5 and RCP8.5. For example, the baseline precipitation of the Dezful Station was small and mostly zero, while this was not the case with the simulations. The same case holds for future temperature projection; while the temperatures of adjacent regions had increasing variations, the temperature variation of the Dezful Station had a reducing trend. Furthermore, the precipitation was found to have small future variations in most central and southern regions in winter and spring, partially due to the fact that the highest annual precipitation occurs in these seasons (over 80% of the annual precipitation). Also, in the southeastern regions with summer precipitation (nearly 11% of the annual precipitation), the variations were small. the western regions have very high future precipitation variations in

summer, partially due to the large temperature difference of summer from the other seasons in the western regions; the summer temperature has a 90% difference from the average annual temperature (summer temperature is equal to the annual average temperature plus 90%). For example, the Hamedan Station has an average baseline annual temperature of 11 °C, while its average summer temperature is 23 °C; the future precipitation variations in autumn with an average temperature of 12 °C were found to be very small. It should be noted that an increase in the temperature increases evaporation into the atmosphere and the probability of rainfall. The comparison of the future annual temperature variations to the baseline period shows that the future temperature is expected to decline in the southern and southeastern regions and rise in the northern
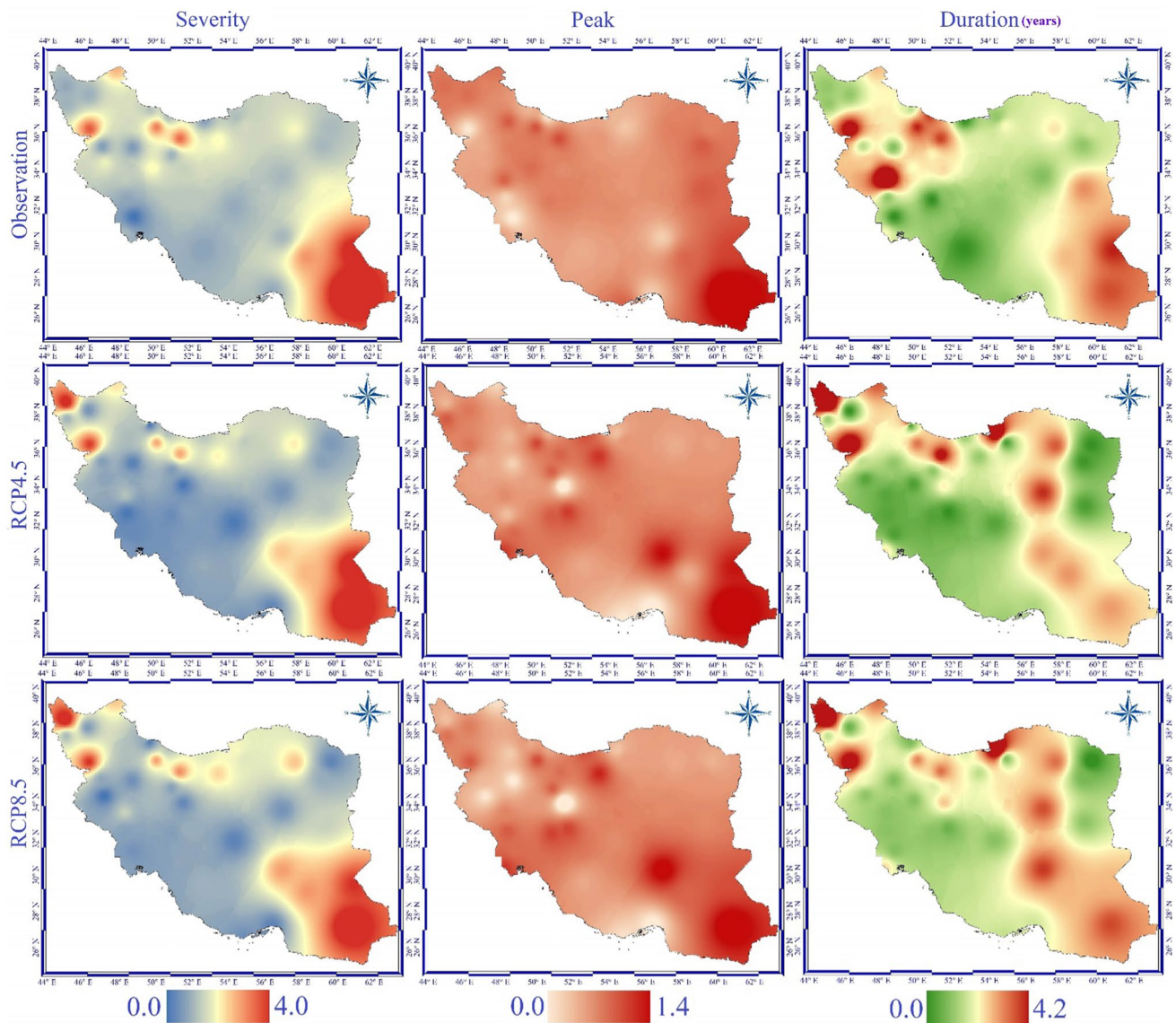
Fig. 10 Spatial distributions of the drought characteristic standard deviations

and northwestern regions. The temperature variations were larger under the scenario RCP8.5. However, some earlier studies indicated an increase in future temperature (Alizadeh-Choobari and Najafi 2018; Asakereh et al. 2020; Doulabian et al. 2021). This can be explained by the fact that the southern, southeastern, and southwestern regions lie in the vicinity of free waters (the Persian Gulf and the Gulf of Oman) and experience smaller temperature differences. Also, these regions have lower latitudes and elevations than the other regions and have different rainfall patterns. In particular, monsoon rainfalls occur in southeastern and southern regions in summer. It should be mentioned that precipitations mostly occur in winter and spring in the majority of Iran, while a majority of

northern precipitations happen in autumn. Moreover, the average baseline seasonal temperature was 10% higher than the average annual temperature in northern and western regions in autumn, while this difference is nearly zero for southern and eastern regions. Furthermore, the average seasonal temperature is lower than the average annual temperature in the southeastern region.

SPI was employed to investigate drought trends for 1, 3, 6, 9, 12, 18, and 24 months. A number of earlier studies reported no trend in long-term drought indices. Zarei and Eslamian (2017) reported a significant trend of the lower-order SPI for the south of Iran and observed that SPI-12 has not any trend duration 1985–2013. Sharafati et al. (2020) demonstrated that SPIs increased for all climates
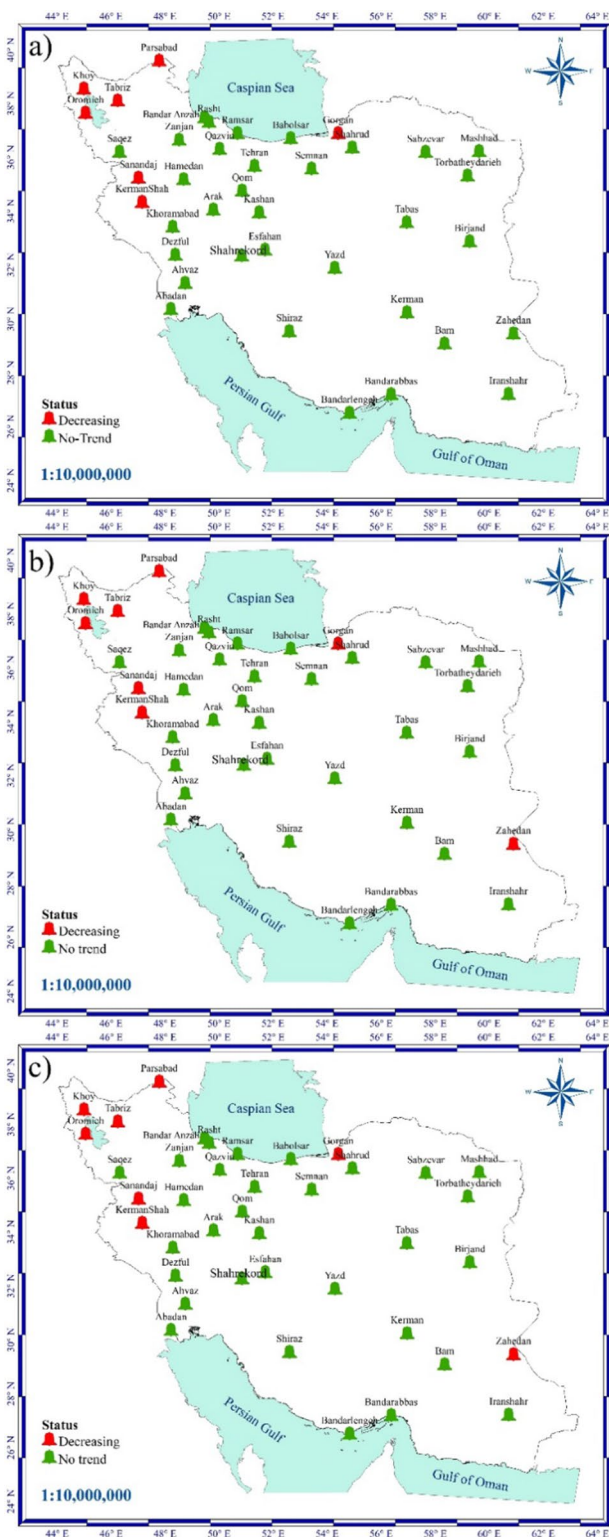
Fig. 11 SPI trend based on the Mann–Kendall test in the baseline and future period (**a** baseline, **b** RCP4.5 and **c** RCP8.5)

for different periods, except for SPI-12. This could have arisen from errors and uncertainty in the data collected in the short-term relative to the long-term data. Furthermore, Sharafati et al. (2020) found an increasing trend of drought in semi-arid and arid climates and a reducing trend in the northwest. Tabari et al. (2012) observed a reducing trend of droughts (increasing drought severity) in the eastern region of Iran. Dashtpagerdi et al. (2015) illustrated a significant rise in the drought severity in the periods of 3, 6, 8, 9, 12, and 24 months at 50% of the 25 stations under study. The droughts mostly occurred in the semi-arid and arid climates of the southern and southeastern of Iran. Golian et al. (2015) evaluated the drought trend in Iran by using SPI during 1980–2013. They observed that drought has a significant trend in the central semi-arid region and arid climates. Abarghouei et al. (2011) analyzed SPI for the periods of 3, 6, 8, 9, 12, and 24 months during 1975–2005. They showed a reducing SPI trend for the southeastern, southwestern, and western regions of Iran and no particular trend for the northern and northeastern parts.

The results of drought analysis indicate that droughts have higher durations and peaks in the southeastern, northern, and northwestern regions in the baseline period. This is also the case with the future period under the scenarios RCP4.5 and RCP8.5, particularly in the northwest. Furthermore, the drought severity has a reducing trend in the northwest. This is consistent with some earlier works. Sharafati et al. (2020) demonstrated that droughts were more severe in the northwest and north. Darand and Sohrabi (2018) described the northwestern part of Iran as a region with the most severe droughts based on daily precipitation variations. Najafi and Moazami (2016) investigated the precipitation trend and the magnitude and frequency of extreme precipitations and showed that the annual precipitation had a reducing trend, particularly in the northern, western, and northwestern parts of Iran.

The drought duration and peak of the stations for the baseline period revealed that the highest drought durations and peaks occurred in semi-arid and arid climates; the stations with semi-arid and arid climates had drought durations of 2–8 years, and the largest drought duration occurred in the southeastern and western stations. Furthermore, the highest drought peaks happened at the northwestern (Parsabad) and southeastern (Iranshahr) stations. This is also the case with the future period; the results suggested higher drought severities in future, and the severities were slightly larger under RCP4.5. The highest future drought durations were found to occur in the northwest (Khoy Station with an arid climate) with a duration of 8 years and southeast (Zahedan, Iranshahr, and Kerman stations with semi-arid climates) with a duration of 6 years. It should be noted that the Gogran Station with a Mediterranean climate will experience 9 years of
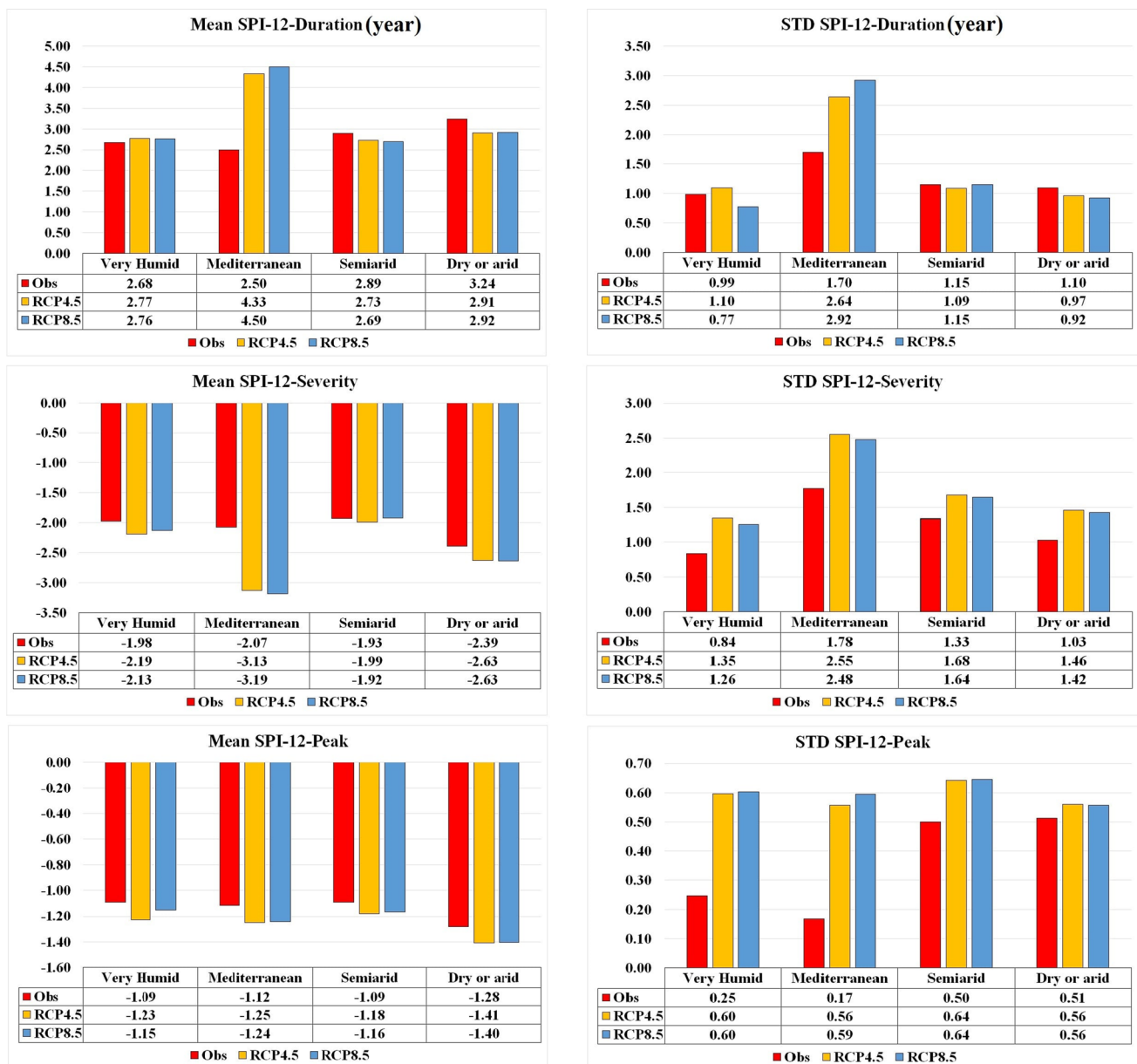
Fig. 12 Standard deviation and mean of drought characteristics (severity, peak, and duration(years)) in different climatic zones

Table 2 Comparison between obtained results with results of other studies in Iran

Study	Description
Najafi & Moazami (2016)	The intensity and frequency of heavy rains have also decreased significantly in the spring season in the northwest region. They showed that the annual precipitation had a reducing trend, particularly in the northern, western, and northwestern parts of Iran
Darand & Sohrabi (2018)	They showed that the northwestern regions and low-altitude areas of Iran with dry and semi-arid climates have the highest probability of drought
Mansouri Daneshvar et al. (2019)	Iran will experience an increase of 2.6 °C in mean temperatures and a 35% decline in precipitation by 2100
Sharafati et al. (2020)	The northwest region of Iran is the most prone to droughts in terms of severity, peak and density
Baghanam et al. (2020)	Simulation for future temperature indicated an ascending trend of 0.1–2.1 °C by 2100 in northwest of Iran
Ghasemi et al. (2022)	They show the decreasing trend for SPI and precipitation at the most of regions of Iran

drought under RCP4.5 and 10 years under RCP8.5 in future; however, drought severity will not be significant.

The investigation of the worst droughts based on SPI at the stations in the baseline period indicated that 5 stations had normal droughts, 18 stations had relatively arid droughts, 11 stations experienced severe droughts, and 6 stations underwent acute droughts. In future period, however, 2(1) stations have normal droughts, 9(12) stations have relatively arid droughts, 15(13) stations experience severe droughts, and 14(14) stations undergo acute droughts under RCP4.5(RCP8.5). Table 2 shows a brief comparison between the results obtained in this study and the results of a number of previous studies.

Conclusion

Although Iran has various climates, arid climates account for the majority of Iran. Based on the De Martonne aridity index and the gridded temperature and precipitation data of the CRU re-analysis database, Iran was classified into arid, semi-arid, Mediterranean, and temperature climates. Then, climate change and meteorological drought were examined in different climates of Iran using the 40-year precipitation and temperature data of 40 synoptic stations. To evaluate climate change, 33 GCMs of IPCC CMIP5 with a spatial resolution of 0.5° were employed. The top ten GCMs of each climate were identified using TOPSIS. The future temperatures and precipitations were projected using the ensembles of the top ten GCMs. The homogeneity of the baseline and future precipitations under the scenarios RCP4.5 and RCP8.5 were examined using SNHT. Due to the greater accuracy of GCMs in long-term projections compared to short-term ones as well as the reduction of computational costs, therefore, the long-term drought was evaluated using SPI-12. The SPI values trends were identified. The variations of the drought characteristics, including severity, peak, and duration, were analyzed. The data were classified based on the climatic characteristics of the stations. Therefore, the innovation in this research is the climatic zoning of Iran and the development of individual and combination models of superior GCMs for simulating temperature and precipitation in each climate zone. This study showed that Iran is divided into four climatic regions based on De Martonne Aridity Index. These four regions are: (a) humid region in the north of Iran (b) Mediterranean region in the northeast and west of Iran (near Iran's border with Iraq and Turkey) (c) semi-arid region in the northwest and west of Iran (d) arid region in the south, center, east and southwest of Iran. In addition, this study showed the top ten GCMs in each climate zone using the TOPSIS method (Fig. 6).

The results showed that the temperature simulation had, in general, higher performance than the precipitation simulation, and temperature uncertainty was lower than precipitation uncertainty due to the conditional nature of precipitation. According to the results, the precipitation of the northern regions had an increasing trend in spring and winter and a reducing trend in autumn and summer. However, the temperature of the northern regions had an increasing trend in autumn and summer and a reducing trend in spring and winter. The comparison of the future annual precipitation variations to those of the baseline period indicated that most stations had reducing future precipitation variations. It was observed that the future precipitations of the central and southern regions would undergo small variations, while the future precipitation variations of the western regions would be very high in summer.

The comparison of the future annual temperature variations to the baseline variations indicated that the south and southeast of Iran will experience reduced temperature, while the northern and northwestern regions will undergo increased temperature, and these variations are larger under RCP8.5. Furthermore, the magnitudes of the future temperature variations are larger in winter, spring, and summer for the northern and southwestern regions. The results showed that the temperature of the northern and western regions in autumn was 10% higher than the average annual temperature, whereas the autumn temperature of the southern and eastern regions was almost the same as the average annual temperature. Also, the southeastern regions were found to have an autumn temperature below the average annual temperature.

The drought severity results demonstrated that the northern and northwestern regions had higher drought durations and peaks in the baseline period. This was also the case with the future period under both scenarios RCP4.5 and RCP8.5, particularly in the northwest where SPI showed a reducing trend in the northwest.

The drought durations and peaks at the stations in the baseline period indicated that the highest drought durations and peaks occurred in semi-arid and arid climates; the semi-arid and arid stations had drought durations of 2–8 years, and the largest drought durations took place at the southeastern and western stations of Iran. Furthermore, the largest peaks occurred at the northwestern and southeastern stations. This is also the case with the future period; the results indicated higher drought severities for the future. In general, the drought severity was slightly larger under RCP4.5. The results revealed future droughts of higher severity, duration, and peaks with larger standard deviations than the baseline period.

The average drought duration results showed that the drought durations of the arid and semi-arid climates were higher than the two other climates in the baseline period.

The average drought duration of Iran was found to be 2.5–3.5 years. The same case holds for the future period.

To examine the drought variation trend, the Mann–Kendall test was employed. The results suggested a reducing drought trend in the northeast (Gorgan station) in the baseline period, while no trend was observed for the other stations. This is also the case for the future period. Also, the southeastern region (Zahedan Station) showed a reducing future trend. Overall, it can be said that the climate of Iran is expected to increase in aridity and semi-aridity in future. As a result, it is necessary to plan and manage water resources, soils, and droughts.

Authors contributions The authors declare that they have contribution in the preparation of this manuscript.

Availability of data and materials All data, models, and code are available from the corresponding author by request.

Declarations

Conflict of interests The authors have no conflicts of interest to declare that are relevant to the content of this article.

Ethical approval The manuscript is an original work with its own merit, has not been previously published in whole or in part, and is not being considered for publication elsewhere.

Consent to Participate The authors have read the final manuscript, have approved the submission to the journal and have accepted full responsibilities pertaining to the manuscript's delivery and contents.

Consent for publication The authors agree to publish this manuscript upon acceptance.

References

Abarghouei HB, Zarch MAA, Dastorani MT, Kousari MR, Zarch MS (2011) The survey of climatic drought trend in Iran. Stoch Env Res Risk A 25(6):851–863. https://doi.org/10.1007/s00477-011-0491-7

Abatzoglou JT, Brown TJ (2012) A comparison of statistical downscaling methods suited for wildfire applications. Int J Climatol 32(5):772–780. https://doi.org/10.1002/joc.2312

Abbasian M, Moghim S, Abrishamchi A (2019) Performance of the general circulation models in simulating temperature and precipitation over Iran. Theor Appl Climatol 135(3–4):1465–1483. https://doi.org/10.1007/s00704-018-2456-y

Adib A, Marashi SS (2019) Meteorological drought monitoring and preparation of long-term and short-term drought zoning maps using regional frequency analysis and L-moment in the Khuzestan province of Iran. Theor Appl Climatol 137(1–2):77–87. https://doi.org/10.1007/s00704-018-2572-8

Adib A, Kisi O, Khoramgah S, Gafouri HR, Liaghat A, Lotfirad M, Moayyeri N (2021) A new approach for suspended sediment load calculation based on generated flow discharge considering climate change. Water Supply 21(5):2400–2413. https://doi.org/10.2166/ws.2021.069

Ahmadianfar I, Zamani R (2020) Assessment of the hedging policy on reservoir operation for future drought conditions under climate change. Clim Change 159(2):253–268. https://doi.org/10.1007/s10584-020-02672-y

Alexandersson H (1986) A homogeneity test applied to precipitation data. Int J Climatol 6(6):661–675. https://doi.org/10.1002/joc.3370060607

Alizadeh-Choobari O, Najafi MS (2018) Extreme weather events in Iran under a changing climate. Clim Dynam 50(1–2):249–260. https://doi.org/10.1007/s00382-017-3602-4

Asakereh H, Khosravi Y, Doostkamian M, Solgimoghaddam M (2020) Assessment of spatial distribution and temporal trends of temperature in Iran. Asia-Pac J Atmos Sci 56(4):549–561. https://doi.org/10.1007/s13143-019-00150-9

Ashofteh PS, Haddad OB, Mariño MA (2013) Climate change impact on reservoir performance indexesin agricultural water supply. J Irrig Drain Eng 139(2):85–97. https://doi.org/10.1061/(asce)ir.1943-4774.0000496

Baghanam AH, Eslahi M, Sheikhbabaei A, Seifi AJ (2020) Assessing the impact of climate change over the northwest of Iran: an overview of statistical downscaling methods. Theor Appl Climatol 141(3–4):1135–1150. https://doi.org/10.1007/s00704-020-03271-8

Bahrami M, Bazrkar S, Zarei AR (2019) Modeling, prediction and trend assessment of drought in Iran using standardized precipitation index. J Water Clim Change 10(1):181–196. https://doi.org/10.2166/wcc.2018.174

Chen C, Greene AM, Robertson AW, Baethgen WE, Eamus D (2013) Scenario development for estimating potential climate change impacts on crop production in the North China plain. Int J Climatol 33(15):3124–3140. https://doi.org/10.1002/joc.3648

Coppola E, Giorgi F, Rauscher SA, Piani C (2010) Model weighting based on mesoscale structures in precipitation and temperature in an ensemble of regional climate models. Clim Res 44(2–3):121–134. https://doi.org/10.3354/cr00940

Darand M, Sohrabi MM (2018) Identifying drought- and flood-prone areas based on significant changes in daily precipitation over Iran. Nat Hazards 90(3):1427–1446. https://doi.org/10.1007/s11069-017-3107-9

Dashtpagerdi MM, Kousari MR, Vagharfard H, Ghonchepour D, Hosseini ME, Ahani H (2015) An investigation of drought magnitude trend during 1975–2005 in arid and semi-arid regions of Iran. Environ Earth Sci 73(3):1231–1244. https://doi.org/10.1007/s12665-014-3477-1

Dlamini T, Songsom V, Koedsin W, Ritchie RJ (2022) Intensity, duration and spatial coverage of aridity during meteorological drought years over northeast Thailand. Climate 10(10):137. https://doi.org/10.3390/cli10100137

Doulabian S, Golian S, Toosi AS, Murphy C (2021) Evaluating the effects of climate change on precipitation and temperature for iran using rcp scenarios. J Water Clim Change 12(1):166–184. https://doi.org/10.2166/wcc.2020.114

Esmaeili-Gisavandani H, Lotfirad M, Sofla MSD, Ashrafzadeh A (2021) Improving the performance of rainfall-runoff models using the gene expression programming approach. J Water Clim Change 12(7):3308–3329. https://doi.org/10.2166/wcc.2021.064

Farajpanah H, Lotfirad M, Adib A, Gisavandani HE, Kisi Ö, Riyahi MM, Salehpoor J (2020) Ranking of hybrid wavelet-AI models by TOPSIS method for estimation of daily flow discharge. Water Supply 20(8):3156–3171. https://doi.org/10.2166/ws.2020.211

Feng S, Hu Q, Huang W, Ho CH, Li R, Tang Z (2014) Projected climate regime shift under future global warming from multi-model, multi-scenario CMIP5 simulations. Global Planet Change 112:41–52. https://doi.org/10.1016/j.gloplacha.2013.11.002

Ghafouri-Azar M, Kim JB, Bae DH (2021) Assessment of the potential changes in low flow projections estimated by Coupled Model Intercomparison Project Phase 5 climate models at monthly and seasonal scales. Int J Climatol 41(5):3222–3236. https://doi.org/10.1002/joc.7015

Ghasemi MM, Mokarram M, Zarei AR (2022) Assessing the performance of SN-SPI and SPI and the trend assessment of drought using the XI correlation technique over Iran. J Water Clim Change 13(8):3152–3169. https://doi.org/10.2166/wcc.2022.176

Gholami H, Lotfirad M, Ashrafi SM, Biazar SM, Singh VP (2023) Multi-GCM ensemble model for reduction of uncertainty in runoff projections. Stoch Env Res Risk A 37(3):953–964. https://doi.org/10.1007/s00477-022-02311-1

Golian S, Mazdiyasni O, AghaKouchak A (2015) Trends in meteorological and agricultural droughts in Iran. Theor Appl Climatol 119(3–4):679–688. https://doi.org/10.1007/s00704-014-1139-6

Hadinia H, Pirmoradian N, Ashrafzadeh A (2017) Effect of changing climate on rice water requirement in guilan, north of Iran. J Water Clim Change 8(1):177–190. https://doi.org/10.2166/wcc.2016.025

Hwang CL, Yoon K (1981) Multiple attribute decision making: methods and applications. Springer, New York. https://doi.org/10.1007/978-3-642-48318-9

Jafarpour M, Adib A, Lotfirad M (2022) Improving the accuracy of satellite and reanalysis precipitation data by their ensemble usage. Appl Water Sci 12(9):232. https://doi.org/10.1007/s13201-022-01750-z

Jeihouni E, Mohammadi M, Eslamian S, Zareian MJ (2019) Potential impacts of climate change on groundwater level through hybrid soft-computing methods: a case study—Shabestar Plain. Iran Environ Monit Assess 191(10):620. https://doi.org/10.1007/s10661-019-7784-6

Kendall MG (1975) Rank correlation methods, 4th edn. Charles Griffin, London

Khaliq MN, Ouarda TBMJ (2007) On the critical values of the standard normal homogeneity test (SNHT). Int J Climatol 27(5):681–687. https://doi.org/10.1002/joc.1438

Lotfirad M, Adib A, Salehpoor J, Ashrafzadeh A, Kisi O (2021) Simulation of the impact of climate change on runoff and drought in an arid and semiarid basin (the Hablehroud, Iran). Appl Water Sci 11(10):168. https://doi.org/10.1007/s13201-021-01494-2

Lotfirad M, Adib A, Riyahi MM, Jafarpour M (2022a) Evaluating the effect of the uncertainty of CMIP6 models on extreme flows of the Caspian Hyrcanian forest watersheds using the BMA method. Stoch Env Res Risk A. https://doi.org/10.1007/s00477-022-02269-0

Lotfirad M, Esmaeili-Gisavandani H, Adib A (2022b) Drought monitoring and prediction using SPI, SPEI, and random forest model in various climates of Iran. J Water Clim Change 13(2):383–406. https://doi.org/10.2166/wcc.2021.287

Maghsood FF, Moradi H, Bavani ARM, Panahi M, Berndtsson R, Hashemi H (2019) Climate change impact on flood frequency and source area in northern Iran under CMIP5 scenarios. Water 11(2):273. https://doi.org/10.3390/w11020273

Mann HB (1945) Nonparametric tests against trend. Econometrica 13(3):245–259. https://doi.org/10.2307/1907187

Mansouri Daneshvar MR, Ebrahimi M, Nejadsoleymani H (2019) An overview of climate change in Iran: facts and statistics. Environ Syst Res 8:7. https://doi.org/10.1186/s40068-019-0135-3

McKee TB, Doesken NJ, Kleist J (1993) The relationship of drought frequency and duration to time scales. In: Proceedings 8th conference applied climatology, American Meteorological Society, Boston, pp 179–184

Mo C, Ruan Y, He J, Jin JL, Liu P, Sun G (2019) Frequency analysis of precipitation extremes under climate change. Int J Climatol 39(3):1373–1387. https://doi.org/10.1002/joc.5887

Modarres R, Sarhadi A, Burn DH (2016) Changes of extreme drought and flood events in Iran. Global Planet Change 144:67–81. https://doi.org/10.1016/j.gloplacha.2016.07.008

My L, Di Bacco M, Scorzini AR (2022) On the use of gridded data products for trend assessment and aridity classification in a Mediterranean context: the case of the Apulia Region. Water 14(14):2203. https://doi.org/10.3390/w14142203

Najafi MR, Moazami S (2016) Trends in total precipitation and magnitude-frequency of extreme precipitation in Iran, 1969–2009. Int J Climatol 36(4):1863–1872. https://doi.org/10.1002/joc.4465

Rahimi J, Ebrahimpour M, Khalili A (2013) Spatial changes of extended De Martonne climatic zones affected by climate change in Iran. Theor Appl Climatol 112(3–4):409–418. https://doi.org/10.1007/s00704-012-0741-8

Sahour H, Vazifedan M, Alshehri F (2020) Aridity trends in the Middle East and adjacent areas. Theor Appl Climatol 142(3–4):1039–1054. https://doi.org/10.1007/s00704-020-03370-6

Sharafati A, Nabaei S, Shahid S (2020) Spatial assessment of meteorological drought features over different climate regions in Iran. Int J Climatol 40(3):1864–1884. https://doi.org/10.1002/joc.6307

Sharma B, Jangle N, Bhatt N, Dror DM (2015) Can climate change cause groundwater scarcity? An estimate for Bihar. Int J Climatol 35(14):4066–4078. https://doi.org/10.1002/joc.4266

Tabari H, Abghari H, Talaee PH (2012) Temporal trends and spatial characteristics of drought and rainfall in arid and semiarid regions of Iran. Hydrol Process 26(22):3351–3361. https://doi.org/10.1002/hyp.8460

Taylor KE (2001) Summarizing multiple aspects of model performance in a single diagram. J Geophys Res Atmos 106(D7):7183–7192. https://doi.org/10.1029/2000JD900719

Thom HCS (1958) A note on the gamma distribution. Mon Weather Rev 86(4):117–122. https://doi.org/10.1175/1520-0493(1958)086%3c0117:ANOTGD%3e2.0.CO;2

Tigkas D, Vangelis H, Tsakiris G (2015) DrinC: a software for drought analysis based on drought indices. Earth Sci Inform 8(3):697–709. https://doi.org/10.1007/s12145-014-0178-y

Vaghefi SA, Mousavi SJ, Abbaspour KC, Srinivasan R, Arnold JR (2015) Integration of hydrologic and water allocation models in basin-scale water resources management considering crop pattern and climate change: Karkheh River Basin in Iran. Reg Environ Change 15(3):475–484. https://doi.org/10.1007/s10113-013-0573-9

Vaghefi SA, Keykhai M, Jahanbakhshi F, Sheikholeslami J, Ahmadi A, Yang H, Abbaspour KC (2019) The future of extreme climate in Iran. Sci Rep UK 9(1):1–11. https://doi.org/10.1038/s41598-018-38071-8

Zamani R, Berndtsson R (2019) Evaluation of CMIP5 models for west and southwest Iran using TOPSIS-based method. Theor Appl Climatol 137(1–2):533–543. https://doi.org/10.1007/s00704-018-2616-0

Zarei AR, Eslamian S (2017) Trend assessment of precipitation and drought index (SPI) using parametric and non-parametric trend analysis methods (case study: Arid regions of southern Iran). Int J Hydrol Sci Technol 7(1):12–38. https://doi.org/10.1504/IJHST.2017.080957

Zhang Y, Long A, Lv T, Deng X, Wang Y, Pang N, Lai X, Gu X (2023) Trends, cycles, and spatial distribution of the precipitation, potential evapotranspiration and aridity index in Xinjiang. China Water 15(1):62. https://doi.org/10.3390/w15010062